Pointing and Tracking Subsystem Design for Optical Communications Link between the International Space Station and Ground

Shinhak Lee, James W. Alexander, and Muthu Jeganathan
Jet Propulsion Laboratory
California Institute of Technology
Pasadena, CA 91109

ABSTRACT

We present a preliminary design for a tracking and pointing subsystem for the optical communication link between the International Space Station (ISS) and a ground receiver at Table Mountain Facility. The link is intended to demonstrate high rate downlink capability of rates up to 2.5Gbps. The design objective of tracking and pointing subsystem is to limit the pointing loss to within 4dB to ensure the maximum downlink capability with 3dB link margin. We will show the underlying tracking and pointing subsystem design and present analysis that shows the allocated error budget can be met.

Keywords: free-space optical communication, tracking and pointing, International Space Station

1. INTRODUCTION

The need for high-speed data communication for space exploration is ever increasing due to increasing scientific and imaging data. For the past several decades, NASA/JPL has been developing high data-rate optical communication technology. Recently, the International Space Station (ISS) Engineering Research and Technology Development program (ISSERT) has sponsored JPL to develop an optical communication terminal whose main objective is to demonstrate high speed down link capability (2.5Gbps) between ISS and a ground receiver, JPL's Optical Communication Telescope Laboratory (OCTL) in 2003. In this paper, we address only the design of the pointing and tracking subsystem. as others are reported separately [2,3].

In Section 2, functional blocks of pointing and tracking subsystem will be described. In Section 3, various pointing errors and error allocation will be presented. In Sections 4 and 5, two major random error sources and simulation results will be discussed in detail. Finally, a summary will be given in Section 6.

2. TRACKING AND POINTING SYSTEM

The pointing and tracking subsystem (Figure 1) is based on the patented laboratory model of the optical Communication Demonstrator (OCD), which has reduced complexity by using a single Focal Plane Array (FPA) and a Fine Steering Mirror (FSM) for all acquisition, tracking, and pointing functions[4]. The improvements in the new design are both advanced FPA and FSM. Due to requirements to have a wide field of view (6mrad), a 512x512 FPA is baselined, which is four times larger than the current OCD FPA (128x128). The increase in format imposes a critical technical challenge in timely readout of the FPA. Given the same frame rate requirement as OCD (two 10x10 subwindows at 2kHz), the need for faster pixel reading requires a new FPA technology such as Active Pixel Sensor (APS) or CMOS sensor that make it possible to implement random access to the region of interest (or subwindow). The requirement on dynamic range was also increased from less than 8bits to 10bits due to tighter pointing accuracy given large atmospheric influences. Also helping to meet the accuracy requirements, the new FSM (LHD design FO-15) has higher open loop bandwidth (500Hz vs. 30Hz). The 0 dB rejection bandwidth from this new FSM is expected to exceed 100Hz.

The tracking and pointing operation is described here: a 980nm beacon is imaged onto a large FPA (512x512) with each pixel covering 12μradx12μrad. Also, a fiber-coupled 980nm laser with 1550nm downlink laser is imaged onto FPA using a retro-reflector. Centroiding of two laser spots with point-ahead information based on the uplink transmitter/downlink receiver generates the driving signal for FSM. The feedback control loop is operated at 2kHz rate. The main differences from OCD are the new FPA and FSM, which will be described in detail in section 4 and 5.

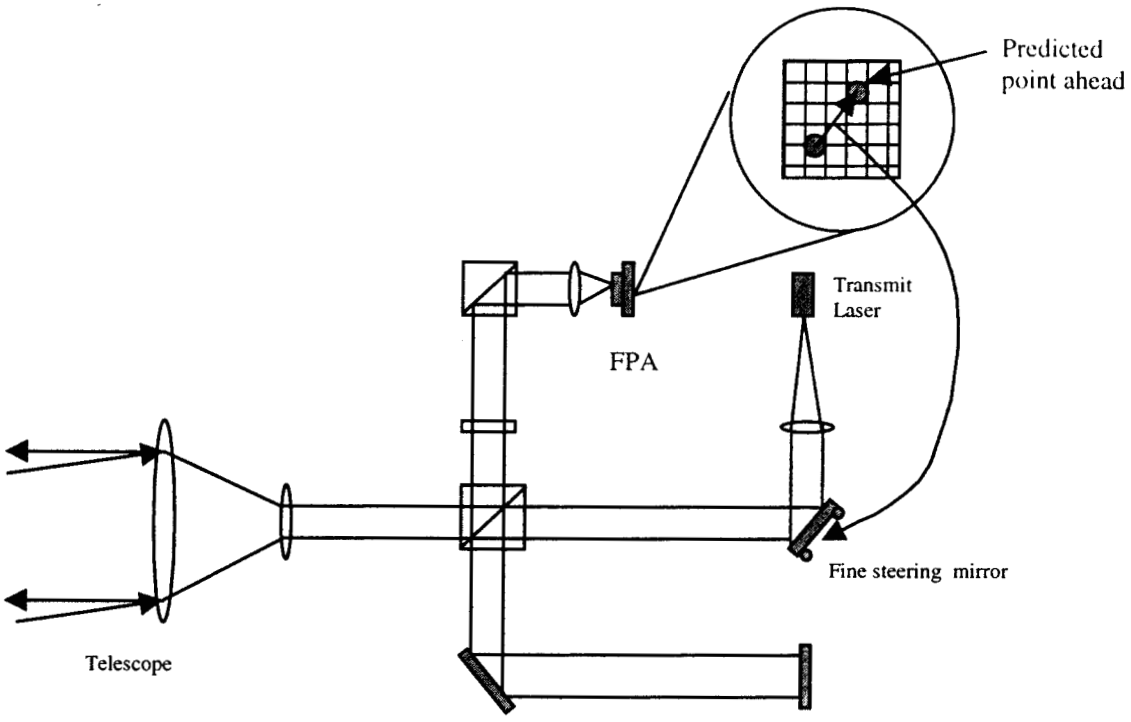

Figure 1. Pointing and Tracking Subsystem

3. POINTING ERROR BUDGET

A minimum link margin of 3dB for 2.5Gbps data rate with negligible pointing fade probability (less than 1%) was established as the fundamental design driver. From this, the overall pointing error budget, 2.3μrad (1 sigma random error) and 2μrad (static error), was established. This overall error consists of various random and static error sources, which are shown in Table 1 with the corresponding error allocations.

Random errors: The two major random error sources are detector (or Focal Plane Array (FPA)) and control system errors. The function of the detector during tracking is to provide relative positions between the laser beacon and downlink transmit beam on the FPA which are then used in the fine steering mirror control loop to point downlink beam to a ground receiver. The estimation of laser beam position is computed using a image centroiding function. The resulting centroiding error (detector error) is a function of signal level, FPA read noise, analog-to-digital converter (ADC) resolution, laser beam profile, FPA non-uniformity FPA fill factor, as well as smear of the image. The allocated errors shown in Table 1 are based on simulation results that will be explained in detail in Section 5. The control system error includes uncompensated error from spacecraft(S/C) and gimbal vibrations. The capability of the control system to compensate for vibrations depends highly on the control loop update rate. Because of the high uplink power available, the frame rate is primarily limited by the readout rate of a FPA. The allocated uncompensated error due to S/C jitter is an estimate based on the predicted closed control loop performance and a preliminary model of S/C jitter [1]. The error from gimbal mis-pointing is rather a requirement that is derived from rough estimate of the currently available gimbal performance.

Static error: The primary static errors are boresight alignment and errors due to thermal and mechanical distortion. Because of the large uncertainty in launch induced misalignments, the majority of the static error, 2μrad, is allocated to alignment error. We assume no post-calibration for this error source. The second error source, point-ahead error, is rather small in this case, which is only 0.05μrad at maximum.

Error Sources	(μrad)	Comments
Detector Error		
Beacon Centroid		
NEA + Pixel to Pixel Nonuniformity	1.05	240,000 e-, 6bits, 2% nonuniformity (1σ)
Spatial Quantization+Intrapixel Nonuniformity	0.50	Simulation result
Transmit Centroid		
NEA + Pixel to Pixel Nonuniformity	0.20	1.3Me-, 6bits, 2% nonuniformity (1σ)
Spatial Quantization+Intrapixel Nonuniformity	0.50	Nominal
Control System Error		
Uncompensated S/C jitter	1.50	Simulation result
Uncompensated Gimbal jitter	1.20	Requirement
Total RMS Jitter (RSS)	**2.30**	

Alignment Error	2.00	
Point Ahead Uncertainty	0.05	
Total Static Error (RSS)	**2.00**	

Table 1. Pointing error allocation table

4. CONTROL SYSTEM ERROR

4.1 ISS VIBRATION ENVIRONMENT

The S/C vibration is the dominant source to the pointing error. Since the gimbal system compensates for the mean motion, the majority of beacon motion on FPA is due to S/C vibration. The corresponding pointing error is therefore proportional to the vibration magnitude. The vibration in high frequency range is a more significant contributor as will be clear when the fine steering control loop is discussed. Therefore, the knowledge of the expected S/C vibration is critical for accurate estimation of pointing error. Currently, the vibration estimation data (Figure 2) on the ISS attach site (S3)[2] is available up to 50Hz. This was generated from finite-element models. Since the effect of S/C vibration should be evaluated over frequency range that influences the pointing accuracy, an appropriate analytical S/C vibration model should be derived. The Olympus S/C vibration model was selected as an approximate analytical model (solid line in Figure 2) which forms an upper bound to the ISS vibration model data. We believe this is a somewhat conservative approach that is seen to be evident from Figure 2, especially in the high frequency region where the difference between the ISS model data and the Olympus S/C vibration model is largest. However, this will give us some extra margin as long as the actual ISS vibration is held below the model data.

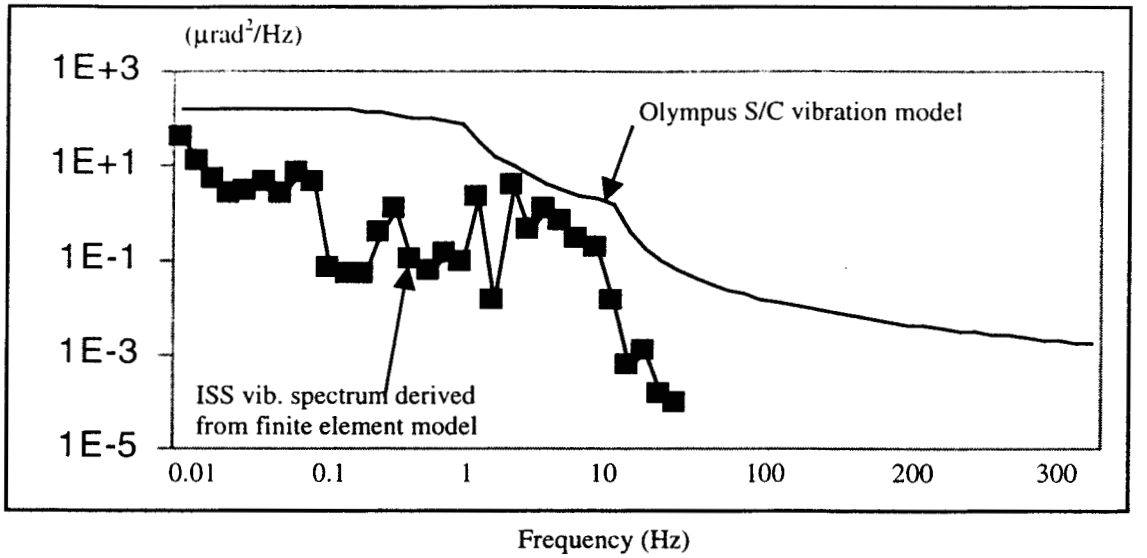

Figure 2. ISS vibration model data vs. Olympus S/C vibration model

4.2 POINTING AND TRACKING CONTROL LOOP

The goal of pointing and tracking control loop is to track the beacon laser using FPA and to point downlink laser to the ground receiver using FSM. The disturbance rejection capability of the control system depends on the controller design, characteristics of FSM and time delay between control loop updates. Since the mirror controller is optimized for the given mirror, the high FSM bandwidth and short time delay result in better rejection capability. For the mirror, we chose the Left Hand Design (LHD) mirror (model FO-15). The open loop characterization of FO-15 can be found in [1]. The new mirror revealed 3dB open loop bandwidth at higher than 500Hz. With the larger open loop bandwidth of the FO-15, we expect the overall rejection performance to improve. With 2kHz control loop updates, the expected disturbance rejection has been previously predicted in [1] and the results shown in Figure 4b. The design of the new controller for FO-15 is currently underway.

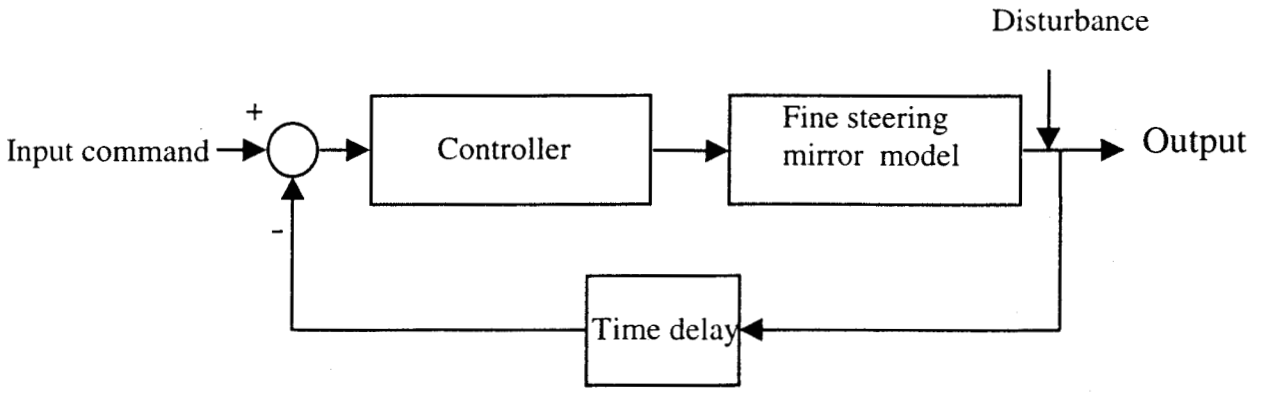

Figure 3. Simplified block diagram of pointing and tracking control system

The corresponding uncompensated error (1.5μrad) from S/C vibration using the Olympus S/C vibration model can be calculated in equation (1) over frequency range of 0 to 300Hz [5]. The uncompensated error from gimbal vibration should be less than 1.2μrad in order to meet the allocated error budget. Without the full knowledge on the vibration spectrum of the gimbal, we have taken the approach of imposing a requirement vibration on the gimbal. This is seen to be readily achievable with gimbal vendor support.

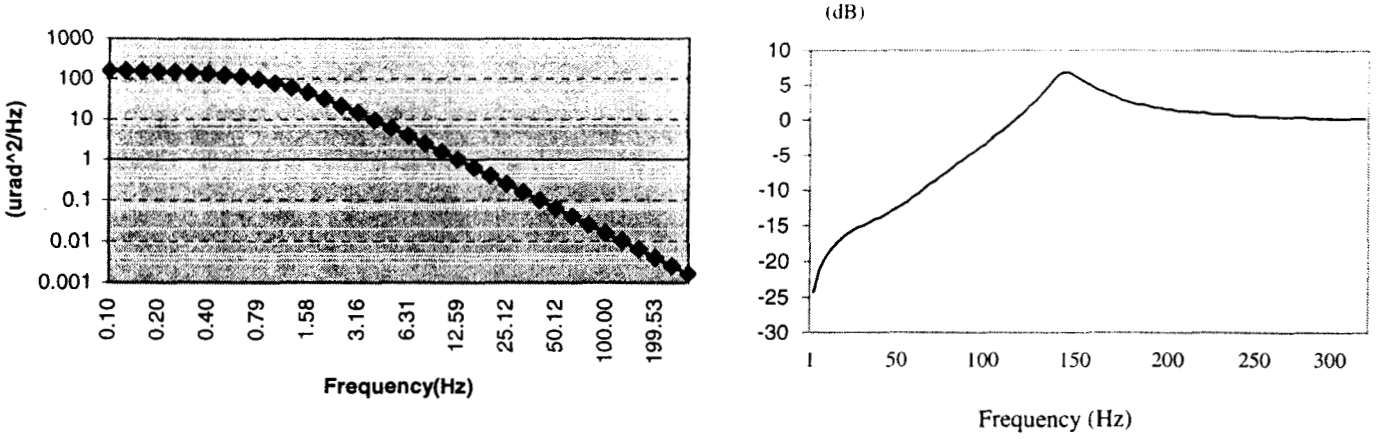

(a) (b)

Figure 4. OLYMPUS S/C Vibration PSD (a), $S(f) = 160/(1+f^2)$ and Tracking Loop Disturbance Rejection (b), R(f).

$$\theta_{rms} = \sqrt{\int S(f) \mid R(f) \mid^2 df} \quad (1)$$
$$= 1.5\mu rad$$

S(f): Angular S/C vibration power spectral density
R(f): Closed loop rejection in the frequency domain

5. DETECTOR ERROR

Detector error is another major random error source and is comprised of several subcomponents. The baseline detector has 512x512 format with a pixel size of 12μmx12μm that covers an angular area of 12μrad square. For the purpose of highlighting the major error sources, we limit our discussions to NEA (Noise Equivalent Angle), pixel-to-pixel nonuniformity, and spatial quantization.

5.1 NOISE EQUIVALENT ANGLE (NEA)

The contributors to NEA include photon shot noise, FPA read noise, dark current, and ADC noise. Figure 5 shows simulation results of NEA based on 9x9 beacon profiles (Figure 7) with 3 different ADC quantization noise levels. The combined noise from read noise and dark current was assumed to be 50e-.

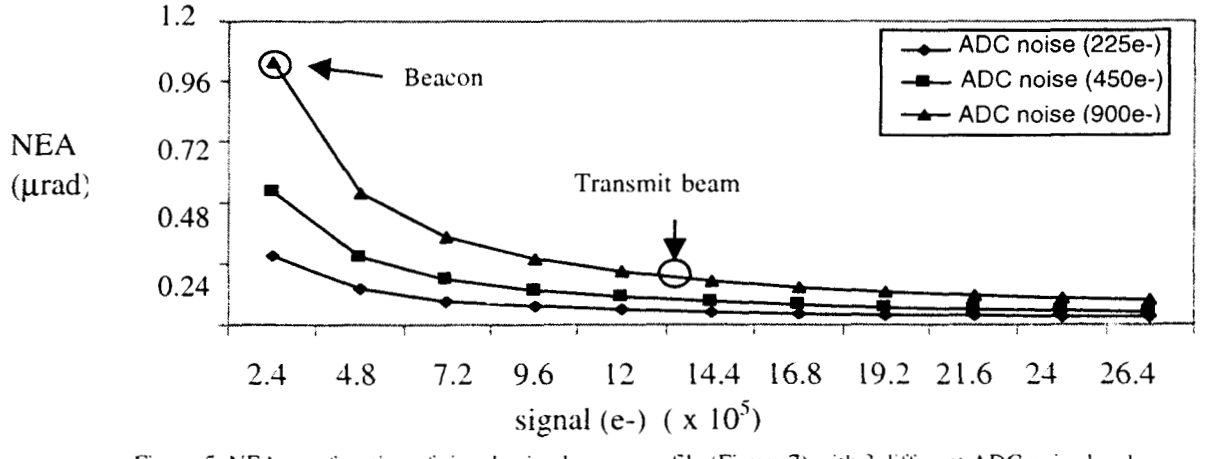

Figure 5. NEA as a function of signal using beacon profile (Figure 7) with 3 different ADC noise levels.

The above results indicate that the allocated error budget of 1.0μrad can be achieved with ADC a resolution of 6 bits and signal level of 240,000e-. For the Earth based transmit beam, the signal level can be easily controlled and 0.2μrad can be achieved with 1.3Me- signal. Since the beacon signal fluctuates due to atmospheric scintillation with dynamic range of more than 10dB, the FPA needs to have an effective resolution range of 10bits.

5.2 PIXEL-TO-PIXEL NONUNIFORMITY

Although the pixel-to-pixel nonuniformity is an important consideration to the pointing error, with no large source of stray-light, the magnitude of error turns out to be rather small. The simulation results in Figure 6 assume the worst case scenario where only the right most column of the centroiding window has different responsivity than the other columns (which here have responsivity of 1). The maximum expected error, given a 2% difference (empirical number for a good detector) in responsivity, is 0.12μrad or approximately 0.04μrad (1 sigma).

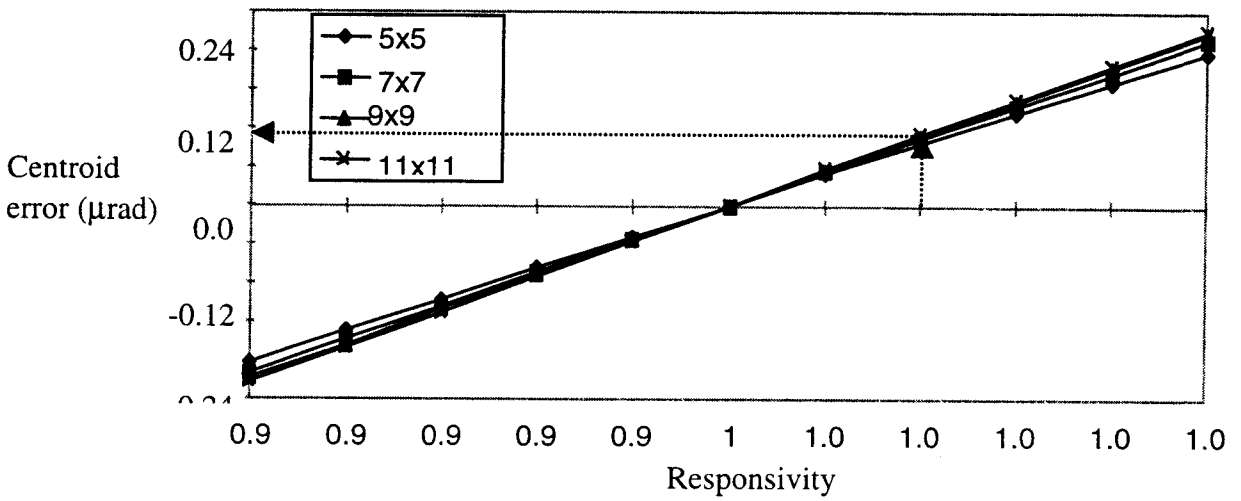

Figure 6. Centroiding error due to nonuniformity of FPA columns

5.3 SPATIAL QUANTIZATION

The centroiding error due to spatial quantization is caused by the finite FPA pixel size and therefore is a function of beam profile, pixel size, and centroiding window size. Unlike NEA, it is a slowly varying bias where the sub-pixel position of the beam spot determines the magnitude of the bias. Generally, centroiding window should be large to reduce spatial quantization error due to truncating the image even though this increases the NEA due to increased pixel noise. Therefore, there should always be a trade-off between these two error sources. Figure 8 shows simulation results on spatial quantization error for 3 different centroiding window sizes given a fixed beam profile (Figure 7). As the results indicate, the larger the centroiding window size, the smaller the centroiding error. However, we can not increase the window size to include the whole beam profiles due to limitations on FPA read rate. Thus, we chose 10x10 as our baseline centroiding window size. The resulting spatial quantization error, 3 sigma of 1.5μrad or 1 sigma error of 0.5μrad satisfies the allocated error budget. In order to obtain the best beam profiles in the centroiding window, the tracking window can be made slightly larger to allow preprocessing such as background subtraction.

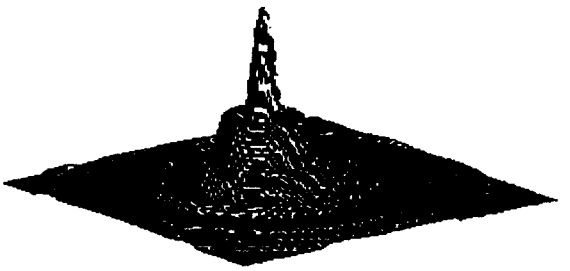

Figure 7. The beacon beam profile at FPA (13x13)

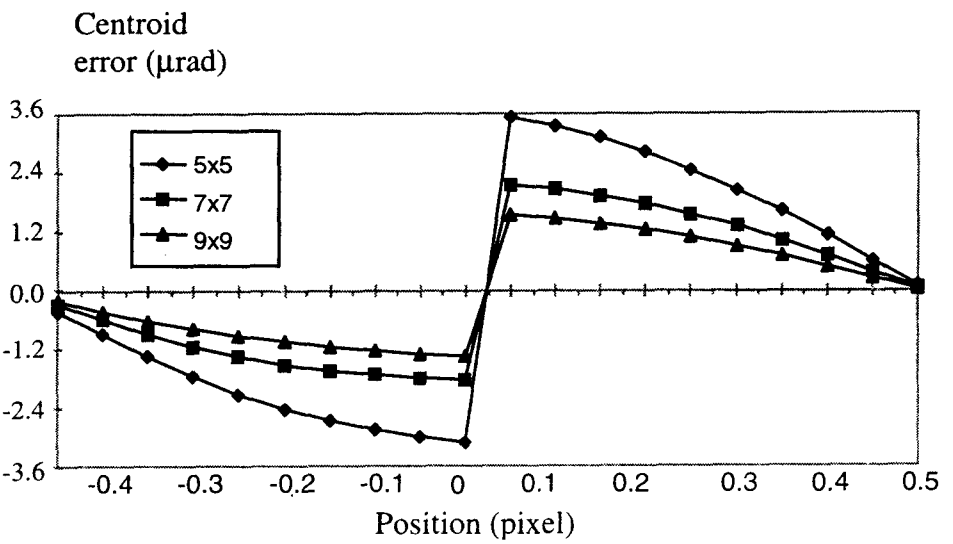

Figure 8. Spatial quantization error on 3 different centroiding window sizes

6. SUMMARY

We presented a preliminary pointing and tracking subsystem design for the ISS-ground link that is intended to demonstrate high speed downlink capability from the ISS to the ground. The baseline pointing and tracking subsystem uses single a FPA and FSM. Simulation results indicated that the objective of limiting pointing loss due to pointing could be achieved using the baseline design. We are now working on designing the mirror controller and implementation of FPAs in our tested.

ACKNOWLEDGEMENT

The research described in this paper was carried out at the Jet Propulsion Laboratory, California Institute of Technology, under contract with the National Aeronautics and Space Administration.

REFERENCES

[1] Caroline Racho and Angel Portillo, "Characterization and Design of Digital Pointing Subsystem for Optical Communication Demonstrator", SPIE Proceedings, *Free-Space Laser Communication Technologies* XI, SPIE, Vol.3615, No.15, San Jose, Jan. 1999.

[2] J. V. Sandusky, M. Jeganathan, G. G. Ortiz, A. Biswas, S. Lee, G. Parker, B. Liu, D. R. Johnson, J. Depew, and J. R. Lesh, "Overview of the preliminary design of the Optical Communication Demonstration and High-Rate Link Facility", *Free-Space Laser Communication Technologies* XI, Proc. SPIE, Vol.3615, 1999.

[3] G. G. Ortiz, M. Jeganathan , J. V. Sandusky, and H. Hemmati, "Design of a 2.5Gbps optical transmitter for the International Space Station", *Free-Space Laser Communication Technologies* XI, Proc. SPIE, Vol.3615, 1999.

[4] M. Jeganathan, A. Portillo, C. S. Racho, S. Lee, D. M. Erickson, J. Depew, S. Monacos, and A. Biswas,"Lessons learned from the Optical Communications Demonstrator (OCD)", *Free-Space Laser Communication Technologies* XI, Proc. SPIE, Vol.3615, 1999.

[5] E. A. Swanson and J. K. Roberge, "Design considerations and experimental results for direct-detection spatial tracking systems", *Optical Engineering* **28**, pp. 659-666, 1989.

[6] C.-C. Chen, J. W. Alexander, H. Hemmati, S. Monacos, T. Y. Yan, S. Lee, J.R. Lesh, and S. Zingles, "System requirements for a deep-space optical transceiver", *Free-Space Laser Communication Technologies* XI, Proc. SPIE, Vol.3615, 1999.

[7] J. W. Alexander, S. Lee, and C.-C. Chen, "Pointing and Tracking concepts for deep-space missions", *Free-Space Laser Communication Technologies* XI, Proc. SPIE,Vol.3615, 1999.